

RESEARCH ARTICLE

Open Access



Mitogen-activated protein kinase signaling causes malignant melanoma cells to differentially alter extracellular matrix biosynthesis to promote cell survival

Anna Afasizheva^{1†}, Alexis Devine^{1†}, Heather Tillman², King Leung Fung¹, Wilfred D. Vieira¹, Benjamin H. Blehm¹, Yorihsa Kotobuki¹, Ben Busby³, Emily I. Chen⁴ and Kandice Tanner^{1*} 

Abstract

Background: Intrinsic and acquired resistance to drug therapies remains a challenge for malignant melanoma patients. Intratumoral heterogeneities within the tumor microenvironment contribute additional complexity to the determinants of drug efficacy and acquired resistance.

Methods: We use 3D biomimetic platforms to understand dynamics in extracellular matrix (ECM) biogenesis following pharmaceutical intervention against mitogen-activated protein kinases (MAPK) signaling. We further determined temporal evolution of secreted ECM components by isogenic melanoma cell clones.

Results: We found that the cell clones differentially secrete and assemble a myriad of ECM molecules into dense fibrillar and globular networks. We show that cells can modulate their ECM biosynthesis in response to external insults. Fibronectin (FN) is one of the key architectural components, modulating the efficacy of a broad spectrum of drug therapies. Stable cell lines engineered to secrete minimal levels of FN showed a concomitant increase in secretion of Tenascin-C and became sensitive to BRAF^{V600E} and ERK inhibition as clonally-derived 3D tumor aggregates. These cells failed to assemble exogenous FN despite maintaining the integrin machinery to facilitate cell-ECM cross-talk. We determined that only clones that increased FN production via p38 MAPK and β 1 integrin survived drug treatment.

Conclusions: These data suggest that tumor cells engineer drug resistance by altering their ECM biosynthesis. Therefore, drug treatment may induce ECM biosynthesis, contributing to *de novo* resistance.

Keywords: Melanoma, Fibronectin, Extracellular matrix, MAPK, Integrin, Tenascin-C, Vemurafenib, Dabrafenib

Background

Molecular studies have determined that aberrant signaling in the mitogen-activated protein kinase (MAPK) signaling cascade (Raf-MEK1/2-ERK1/2) is a crucial step in melanocytic neoplasia, ultimately deregulating the activity of key transcription factors that control cell growth, differentiation, and survival [1]. Specifically, gain of function mutations in which the 600 valine residue of

the BRAF kinase is substituted with glutamic acid (BRAF^{V600E}) are present in ~40 % of patients presenting with malignant melanoma [2]. Survival is enhanced if detection, treatment and surgical excision occur when the tumor burden is restricted to a primary site; however, once the disease has metastasized to distant organs such as the lung, brain, bone, and liver, prognosis is poor, with a median survival of ~9 months [3]. These dismal statistics are in part due to the intrinsic resistance of melanoma to platinum-based chemotherapeutics and its rapid acquisition of resistance to initial therapeutic interventions [4, 5]. Present treatment strategies involve small molecule inhibitors of this mutant BRAF kinase,

* Correspondence: kandice.tanner@nih.gov

†Equal contributors

¹Laboratory of Cell Biology, Center for Cancer Research, National Cancer Institute, National Institutes of Health, 37 Convent Dr., Bethesda, MD 20892, USA

Full list of author information is available at the end of the article



such as vemurafenib and dabrafenib [6, 7]. However, these therapies are only effective in a subset of patients: those that harbor the more prevalent BRAF^{V600E} and the less common BRAF^{V600K} mutations [8]. While drugs targeting this specific isoform are among the most promising melanoma treatments, patients eventually relapse due to reactivation of the MAPK signaling cascade, specifically ERK activity [5, 9]. To overcome *de novo* resistance, a combinatorial treatment of vemurafenib with a MEK inhibitor is administered in an effort to combat reactivation of the MAPK pathway [10–12]. However, mechanisms that underlie acquired resistance after treatment with multiple inhibitors of this pathway remain elusive.

Drug resistance has been shown to be mediated by tissue architecture and cell-adhesion [13, 14]. In particular, cell adhesion-mediated drug resistance (CAM-DR) is an emergent phenotype associated with cell-cell adhesion or 2D adhesion to extracellular matrices. Myeloma cells cultured as monolayers that had adhered to fibronectin were resistant via upregulation of $\alpha 4 \beta 1$ integrin compared to cells treated in suspension [15]. Similarly, tumor cells grown as spheroids show increased resistance to therapy compared to the same cells that are dissociated and grown as monolayers [16]. However, the observed acquired drug resistance following multiple targeting of the MAPK pathway is not readily explained by CAM-DR [12]. Because this reactivation attenuates drug response, it may also contribute to the development of acquired resistance [12].

The tumor microenvironment is emerging as a critical factor in malignant progression, metastasis and tumor etiology [17, 18]. To explore mechanisms that drive tumors to overcome and survive under unfavorable conditions, we aimed to delineate tumor-induced microenvironmental responses to the stress induced by drug therapeutics. Tumor cells actively modulate the host environment by secreting cytokines that reprogram stromal cells to change the extracellular matrix (ECM) milieu, thus creating a *de novo* microenvironment [17, 18]. While immunotherapy and monoclonal antibodies targeting tumor angiogenesis have shown promising results, many microenvironmental targets remain underexplored [18]. For example, overexpression of secreted ECM proteins such as fibronectin (FN) has been found in several solid carcinomas, and postulated to be beneficial for tumor growth and instrumental in the establishment of an ideal microenvironment [19]. Furthermore, heterogeneous expression of ECM components within tumors has been observed [20]. Pathologists have long associated the presence of abundant ECM proteins in tumors with poor prognosis and an expected dismal response to therapeutic intervention [21].

Recently, a study showed that non-small cell lung cancer cells induced FN biogenesis via p38 MAPK in response to treatment with cetuximab (targeting the EGF receptor upstream of the MAPK signaling pathway) [22]. This response was found to blunt the cytotoxic effects of cetuximab and reduced sensitivity to radiotherapy in *in vitro* and *in vivo* murine models. FN biogenesis may also reduce the efficacy of drugs targeting the BRAF kinase. Earlier observations found that a cocoon of ECM proteins, including FN, laminin, collagen IV and Tenascin C, protect small lung cancer cells from chemotherapy-induced apoptosis [23]. We hypothesized that melanoma cells modulate secretion of not only FN, but also other ECM molecules to survive drug treatment. An important question is whether baseline ECM expression *per se* can predict cell survival and drug resistance. Furthermore, is upregulation of ECM proteins a reaction to evolutionary pressure following drug treatment, the result of selection for pre-existing resistant subpopulations, or a combination of both? Seeking to identify and determine the temporal regulation of the secreted ECM proteins, we focused on two isogenic cell lines to mimic intratumoral heterogeneity. Our results indicate that tumor cells adjust their 3D microenvironment by modulating secretion of FN and Tenascin-C (TNC), thereby blunting the effects of MAPK pathway inhibition. We show that only clones that can modulate their ECM secretion in response to pharmaceutical stress survive. Mechanistically, FN biogenesis via p38 MAP kinase via $\beta 1$ integrin is induced following pharmaceutical treatment of the MAPK signaling pathway. Also, our data suggests that biogenesis of TNC is an possible alternative to impaired FN production. This study indicates a critical role for *de novo* ECM biogenesis as a mechanism driving acquired resistance to drugs targeting MAPK signaling in cutaneous melanoma.

Methods

Human melanoma cell lines, A375 (cat. No. CRL-1619) and A375.S2 (cat. No. CRL-1872) cells were obtained from American Type Culture Collection (ATCC, Manassas, VA) and cultured on tissue culture flasks as described by the ATCC. A375 and A375.S2 cells were grown as monolayers in DMEM high glucose media (Life Technologies, Carlsbad, CA) supplemented with final volume of 10 % Fetal Bovine Serum (FBS), 1 % MEM non-essential amino acids, L-Glutamine, Penicillin and Streptomycin. Cells cultured with the media was refreshed every 2-3 days.

Animal studies

Animal studies were conducted under protocols approved by the National Cancer Institute, and the National Institutes of Health Animal Care and Use Committee. Briefly, 5×10^5 A375 cells were injected via

tail vein into 8–10-week old female nu/nu mice. Three weeks after injection mice were euthanized and lungs were extracted and inflated and fixed in 4 % paraformaldehyde solution for 12 h and then prepared for histological staining. Lungs were then embedded in paraffin prior to sectioning on a microtome. Following antigen retrieval using xylene, samples were rehydrated and serial sections; 8 μ m thick were labeled for specific stains of human fibronectin and DAPI.

Human tissue arrays and RNAseq

Human tissue arrays (cat # T386) were purchased from US Biomax (US Biomax, Rockville, MD) where tissue biopsies of human normal skin, melanoma with and without metastasis were examined by immunofluorescence. Briefly, antigen retrieval using xylene as described for mouse tissue was conducted and following re-hydration. Samples were stained for human Fibronectin and DAPI. Public RNAseq datasets were submitted to National Center for Biotechnology Information (NCBI) and examined for expression of extracellular matrix proteins [24] and a search was done for public studies that involved ECM in melanoma (<http://www.ncbi.nlm.nih.gov/pubmed/?term=tenascin%20C%20AND%20melanoma>).

Briefly, normal melanocyte cell lines were compared to melanoma cell lines. In addition, data before and after treatment in human patients were also mined from publicly available databases.

3D cell culture

Cells were seeded at a concentration of 2×10^5 cells per ml of Matrigel (BD Biosciences, San Jose, CA), which polymerized to form a hydrogel at 37 °C. Media was added to the hydrogels after 30 min to ensure complete gelation. Cells were harvested after growth in 2D and embedded in laminin-rich extra cellular matrix (lrECM) (BD Biosciences) at 37 °C, in 5 % CO₂ as previously described [25]. Clonally derived multicellular aggregates were examined 10 days later for morphology and protein analysis.

Conditioned media collection and protein preparation

For 2D culture, cells were seeded at 5×10^5 cells per well in a six well plate with regular media. After 24 h the regular media was removed and cells were washed twice with PBS, and serum-free media was added. Conditioned (serum-free) media and cell lysate were collected after 24 h. For 3D culture, cell washing and refresh with conditioned medium was conducted repeated at day 8, following sample collection at day 9. For 3D cultures, cells were also harvested from lrECM for immunoprecipitation as previously described [25]. Melanoma cells and normal human melanocytes were lysed in Mammalian Protein Extraction Reagent (Thermo Scientific, Waltham, MA), 1 \times protease inhibitor cocktail

(Calbiochem, Billerica, MA) and 1 \times phosphatase inhibitor cocktail 2 & 3 (Sigma-Aldrich, St. Louis, MO) followed by centrifugation (13,200 rpm, 4 °C, 5 min), after which the supernatants were stored at -80 °C until use. Protein concentrations were determined with the Pierce[®] BCA Protein Assay kit (Thermo Scientific), using BSA as the concentration standard. Extracted proteins were then resolved using 4–12 % Bis-Tris Gels (Life Technologies) and subsequently transferred to PVDF membranes (Life Technologies) for immunoblotting.

Western blot analysis

PVDF membranes were washed and blocked with 1 % BSA in TBS (20 mM Tris-HCl, 150 mM NaCl, pH 7.4) containing 0.1 % Tween-20 (TBS-T) and incubated with the primary antibodies. Next, the membranes were incubated with horseradish peroxidase-conjugated donkey anti-rabbit IgG (GE Healthcare, Buckinghamshire, UK) or sheep anti-mouse IgG (GE Healthcare). Finally, the immunoblot was incubated with an enhanced chemiluminescence (ECL) reaction system (Invitrogen) and the ECL signals were visualized by film. The antibodies were used at the following dilutions: anti-FN (1:1,000), anti- α integrin (1:1,000), anti- β 1 integrin (1:1,000), anti-phospho-p44/42MAPK (1:1,000), anti-p44/42MAPK (1:1,000), and anti-GAPDH (1:2,000). Except anti-FN (Origene, Rockville, MD), antibodies are purchased from Cell Signaling Technology (Danvers, MA).

RNA extraction, reverse transcription, and RT-PCR

Total RNA was extracted using an RNeasy mini Kit (Qiagen, Valencia, CA) and first-strand complementary DNAs (cDNAs) were synthesized from 500 ng of each total RNA preparation with the Quantitect Reverse Transcription kit (Qiagen) according to the manufacturers' instructions. The PCR products were detected by SYBR Safe DNA gel stain (Invitrogen) after separation in 1 % agarose gel. β -actin was used as a housekeeping gene to evaluate and compare the quality of different cDNA samples. The primer sequences and the expected sizes of PCR products were as follows: Human FN 1, forward, 5'-ACAGGAAAGAGATGCGCCAA-3', reverse, 5'-GGAAGAGTTTACGGGGTCC-3' (403 bp); Human β -actin, forward, 5'-AGCCTCGCCTTTGCCGA-3', reverse, 5'-CTGGTGCCTGGGGCG-3' (174 bp). AmpliTaq Gold with GeneAmp and dNTP Mix (Applied Biosystems, Branchburg, NJ) were used for the RT-PCR analysis. We used a denaturing step of 94 °C for 5 min, followed by a cycling program of 94 °C for 10 s, 58 °C (Human FN1) or 60 °C (Human β -actin) for 60 s, and 72 °C for 60 s for 40 cycles, and a final holding stage at 4 °C.

Materials for mass spectroscopy

Dithiothreitol (DTT), acetonitrile (ACN), ammonium bicarbonate, trifluoacetic acids (TFA), and iodoacetamide

(IAA) were from Thermo Fisher Scientific. Trypsin Gold, mass spectrometry grade, was from Promega (Madison, WI). Nanopure water was prepared with use of Milli-Q water purification system (Millipore, Billerica, MA).

Preparation for in-gel protein digestion

For MS analysis, cells were grown in 1 % dialyzed FBS in 10 cm dishes and conditioned media (CM) collected every 2 days; protease and proteinase inhibitors were added immediately. CM was centrifuged at 3,500 rpm for 30 min to remove cell debris and the supernatant was concentrated using Amicon Ultra-15, Ultracel-3 K (ThermoFisher, Cat No: UFC900324) following the manufacturer's instructions until the volume was reduced to ~300ul. Protein concentration was determined using BCA assay. 30 µg of proteins were separated using pre-cast 4–20 % Tris-Glycine SDS-PAGE gels (Life Technologies). Total protein resolved in the polyacrylamide gel was stained with Coomassie blue (Sigma). The gel was destained, reduced, alkylated, and dried for in-gel digestion. Biological replicates at each time point ($n = 3$) were run on the same gel and processed simultaneously.

In-gel protein digestion

The dried gel pieces were rehydrated and digested in 80 µL of 12.5 ng/µL Trypsin Gold/50 mM ammonium bicarbonate at 37 °C overnight. After the digestion was complete, condensed evaporated water was collected from tube walls by 5 s centrifugation using a benchtop microcentrifuge (Eppendorf, Hauppauge, NY). The gel pieces and digestion reaction were mixed with 50 µL 2.5 % TFA and rigorously mixed for 15 min. The solution with extracted peptides was transferred into a fresh tube. The remaining peptides were extracted with 80 µL 70 % ACN/5 % TFA mixture using rigorous mixing for 15 min. The extracts were pooled and dried to completion (1.5–2 h) in SpeedVac. The dried peptides were reconstituted in 30 µL 0.1 % TFA by mixing for 5 min and stored in ice or at -20 °C prior analysis.

LC-MS/MS analysis

Samples were centrifuged at 14,000–16,000 × *g* for 10 min to remove particulate material. Five microliters of each sample were injected into a self-packed fused silica nano column, which had been pulled to a 5 µm i.d. tip using a P-2000 CO₂ laser puller (Sutter Instruments, Novato, CA), then packed with 13 cm of 3 µm C18 reverse phase (RP) particles (Magic C18 AQ 3 µm (Michrom. Bioresources, Auburn, CA)) and equilibrated in 5 % acetonitrile, 0.1 % formic acid. Full MS spectra were recorded on the peptides over a 400 to 2000 *m/z* range by the Orbitrap, followed by five tandem mass (MS/MS) events sequentially generated by LTQ in a data-dependent manner on the first, second, third, and fourth most intense ions

selected from the full MS spectrum (at 35 % collision energy). Mass spectrometer scan functions and HPLC solvent gradients were controlled by the Xcalibur data system (Thermo Finnigan, San Jose, CA).

Database search and interpretation of MS/MS datasets

Tandem mass spectra were searched against a concatenated target-decoy database containing the forward and reverse sequences of the target database using the Proteome Discoverer 1.4 and SEQUEST search engine (Thermo Finnigan). The target sequence was downloaded from a human Uniprot database (database released on November 13, 2013) and 124 common contaminant proteins. The search algorithm was configured to specify the following parameters: precursor tolerance, 10 ppm; fragment tolerance, 0.5 Da; static modification, cysteine carbamidomethylation; and fully tryptic status. SEQUEST search results from Proteome Discoverer were further analyzed by Scaffold (Proteome Software Inc., Portland, OR). The discriminant score was set such that a false positive rate of 1 % was determined based on the number of accepted decoy database peptides. Scaffold outputs label-free quantification based on precursor ion intensity for data from Proteome Discoverer. Precursor intensity refers to the area under an MS1 spectrum peak corresponding to a specific peptide. We used normalized total precursor intensity to derive quantitative values in this paper. Statistical analysis was performed by Qlucore Omics Explorer (Qlucore AB, Lund, Sweden). Two group comparisons (a paired *t*-test) was used to compare the mean value of relative abundance based on normalized total precursor intensity from three biological replicates for each protein identified in conditioned media collected in day 2 and day 10. The heatmap was generated based on hierarchical clustering of global protein expression filtered by the *p*-value ($p < 0.05$).

Cell growth inhibition assay by MTT method

Cellular toxicity to drugs was measured by the MTT (3-(4,5-Dimethylthiazol-2-yl)-2,5-diphenyltetrazolium) method or CCK-8 (Dojindo Molecular Technologies, Inc., Rockville, MD) method following manufacturer's instructions.

Generation of shFN1 and shFN2 stable cell lines

Plasmids encoding FN knockdown shRNAs were isolated from Mission shRNA Bacteria Glycerol Stocks NM_002026/TRCN0000293839 and NM_002026/TRCN0000293840 (designated shFN1 and shFN2, respectively). MISSION[®] pLKO.1-puro Non-Mammalian shRNA control plasmid (SCH002, Sigma) was amplified in MAX Efficiency[®] DH5α[™] Competent Cells (Invitrogen) for 16 h at 30 °C. Plasmids were extracted from ampicillin-supplemented LB liquid cultures amplified

from single colonies over 16 h at 30 °C using Qiagen Plasmid Midi Kit. Individual plasmids were co-transfected with lentiviral packaging plasmids (Invitrogen) into 293FT cells by Fugene6 Transfection Reagent (Roche, Basel, Switzerland). Viral supernatant was harvested after 48 and 72 h and concentrated by ultracentrifugation at 26,000 rpm through a 20 % sucrose gradient.

Lentiviral transduction

Melanoma cells were transduced with virus using ExpressMag Transduction System (Sigma). Briefly, viral supernatant was incubated with magnetic beads at room temperature for 15 min, added to the adherent cells and placed on a strong magnetic plate at 37 °C for 12 min. Media was replenished 16 h later and the viral mixture disposed in compliance with NIH policy. Transduced cells were selected with 2 µg/ml puromycin (InvivoGen, San Diego, CA).

Immunofluorescence

For examination of 2D culture, cells were seeded directly onto glass chambers with a coverslip-bottomed no. 1.0, (Nalge, Nunc) according to previously described methods [25]. For 3D interrogation, samples were prepared as previously described [25]. Samples were rinsed twice with PBS, fixed with 4 % paraformaldehyde solution for 20 min, permeabilized with 0.5 % Triton X-100 for 20 min and rinsed and blocked in 5 % horse serum for 1 h at room temperature. Cells were then incubated with anti-FN1 antibody (1:100) and anti-actin antibody (1:100) for 12 h at 4 °C in 5 % horse serum. After incubation with primary antibody, cells were rinsed three times with PBS and then incubated with secondary antibodies (1:200) for 2 h at 4 °C. Cell nuclei were stained with DAPI (Sigma). Images were acquired with an upright Zeiss LSM 780 Meta confocal microscope (Zeiss, Jena, Germany).

Imaging specifications

One-photon, confocal, 2-dimensional images of 512 × 512 pixels (lateral dimensions) were acquired with a 1.4 NA 40 × oil-immersion objective. We sequentially excited our sample with the 405 nm, 488 nm lines from an argon ion laser with a power of < 3 % (total power 30 mW) and 546 nm from a solid-state laser (power of < 10 %). A secondary dichroic mirror, SDM 560, was employed in the emission pathway to delineate the red (band-pass filters 560–575 nm) and green (band-pass filters 505–525 nm) and blue channels (480–495 nm) at a gain of 400 on the amplifier. The laser power for the 543 nm setting was set at < 3 % of the maximum power and the gain on the detectors was set to 450.

3D soft agar assay

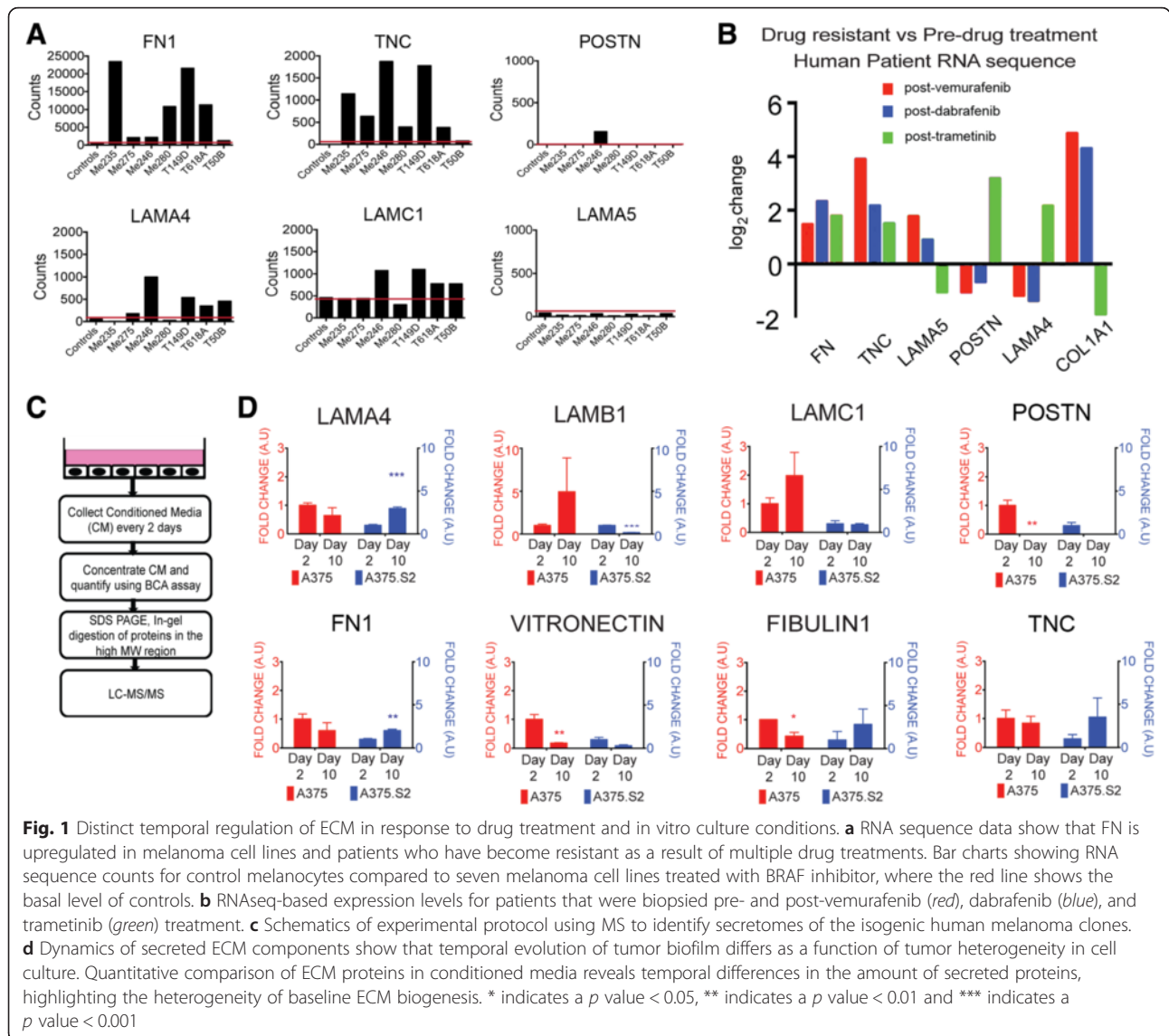
Anchorage-independent proliferation was quantified by soft agar assay. Cells were suspended in 1 mL of 0.36 % (w/v) bacto-agar (BD Biosciences) overlaid by a 0.6 % (w/v) bacto-agar support in 6-well plates in triplicates at densities of 5×10^3 cells per well for A375, A375.S2, A375Scr, A375 shFN2, A375.S2 Scr, A375.S2 shFN2 lines, respectively. Plates were incubated at 37 °C in normoxic conditions. Pathway inhibitors were used at the following concentrations: 3.0 µM cisplatin (DNA-cross-linking agent), 3.0 µM VX-11e (ERK inhibitor), 3.0 µM vemurafenib (BRAF^{V600E} inhibitor) (Chemietek, Indianapolis, IN), and 50 nM paclitaxel (microtubule stabilizing agent) (Life Technologies). Pathway inhibitors were administered at the beginning of the experiment or initiated 14 days later. At the end of the experiment, wells were stained with 0.5 µg/mL of nitroterazolium blue chloride (Sigma-Aldrich). Colonies with > 20 µm in diameter were counted using the Bioreader Software and a BioSys BioCount 4000 Pro machine. Clonogenic survival for each line and condition was plotted as frequency of colony size normalized to a gaussian distribution. Experiments were performed in triplicate.

Results

Distinct temporal regulation of extracellular matrix protein production in response to drug treatment is dynamic

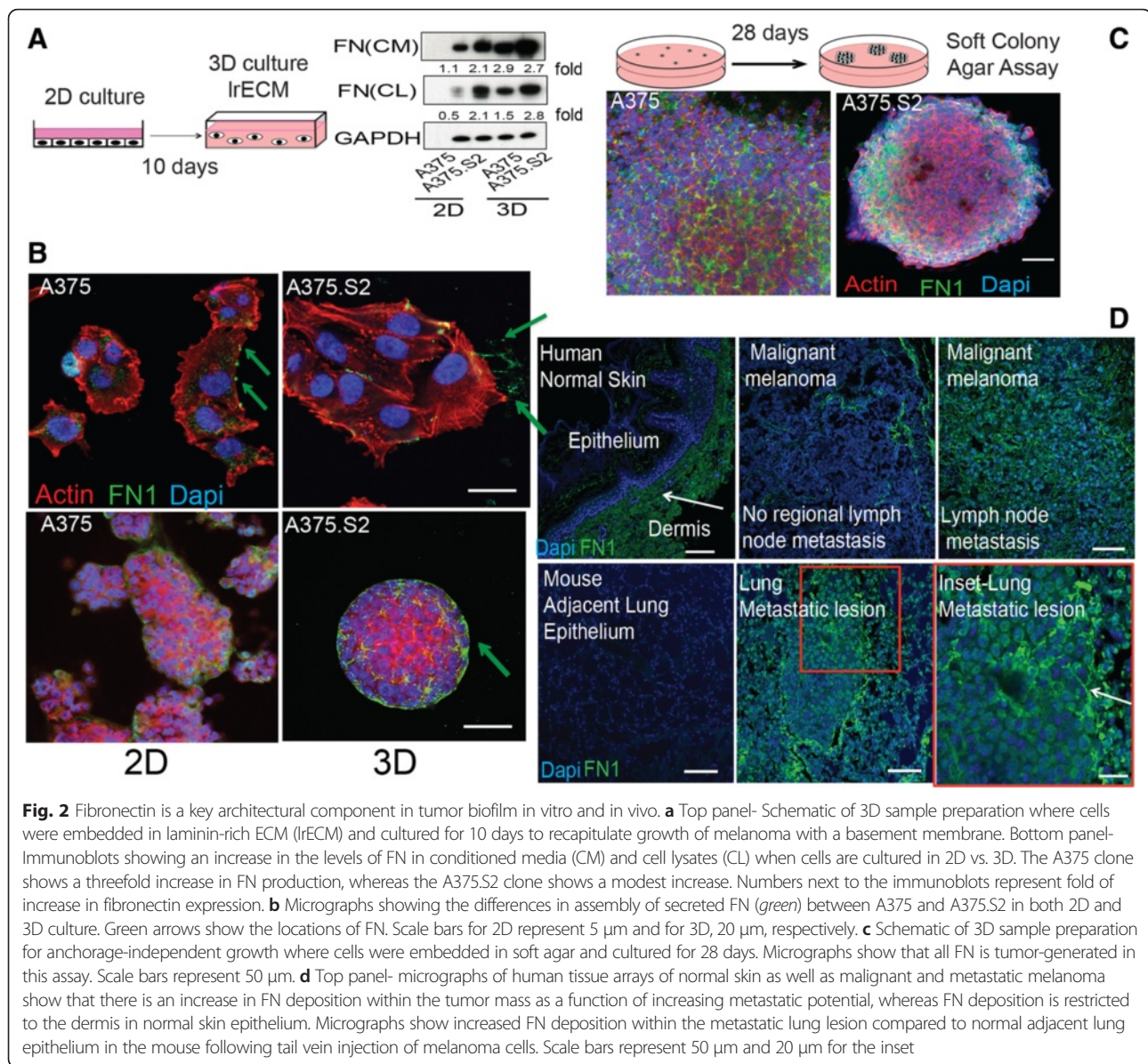
Public RNAseq datasets submitted to National Center for Biotechnology Information (NCBI) were examined for expression of extracellular matrix proteins. Six melanoma cell lines consistently showed higher expression of FN1 (fibronectin) than pooled human melanocyte controls (Fig. 1a) [24]. The only other known ECM-related transcript consistently upregulated at the RNA level was TNC (Tenascin-C), which has been shown to be involved in melanoma progression [26]. Moreover, when a separate dataset was examined for RNAseq-based expression levels in human patients, pre- and post-vemurafenib (first column), dabrafenib (second column) and trametinib (third column) treatment, the same pattern of expression (presented as log₂ (control)) was observed, with FN1 and TNC, but not other ECM-related transcripts, consistently upregulated at the RNA level [27] (Fig. 1b). This may occur in response to treatment, or due to selective survival of tumor cells that originally expressed higher levels of the ECM.

To determine the dynamic contributions made by tumor cells to the establishment of a *de novo* tumor microenvironment, we selected A375 and its derivative clone A375.S2, which are isogenic human melanoma cell lines that reflect established intratumoral heterogeneity. These cell lines harbor a BRAF^{V600E} mutation and are



tumorigenic when injected into immune-compromised mice. Using a tandem mass spectrometry-based technique (LC-MS/MS), we analyzed the culture media conditioned by the parent and its derivative cell lines over the course of 10 days in 2D culture (Fig. 1c). We identified many ECM-related proteins were commonly or differentially secreted. The amount of these secreted ECM components was modulated as a function of time, thus illustrating the dynamics of tumor biofilm formation, and baseline secretion was also consistently distinct between the clones (Fig. 1d). Secretion of fibronectin (FN), in particular, varied significantly in amount and timing in A375 and A375.S2 cell lines. We thus reasoned that using the 3D biomimetic platforms, we could further address the heterogeneity of ECM secretion and dynamics, particularly as it relates to acquired resistance.

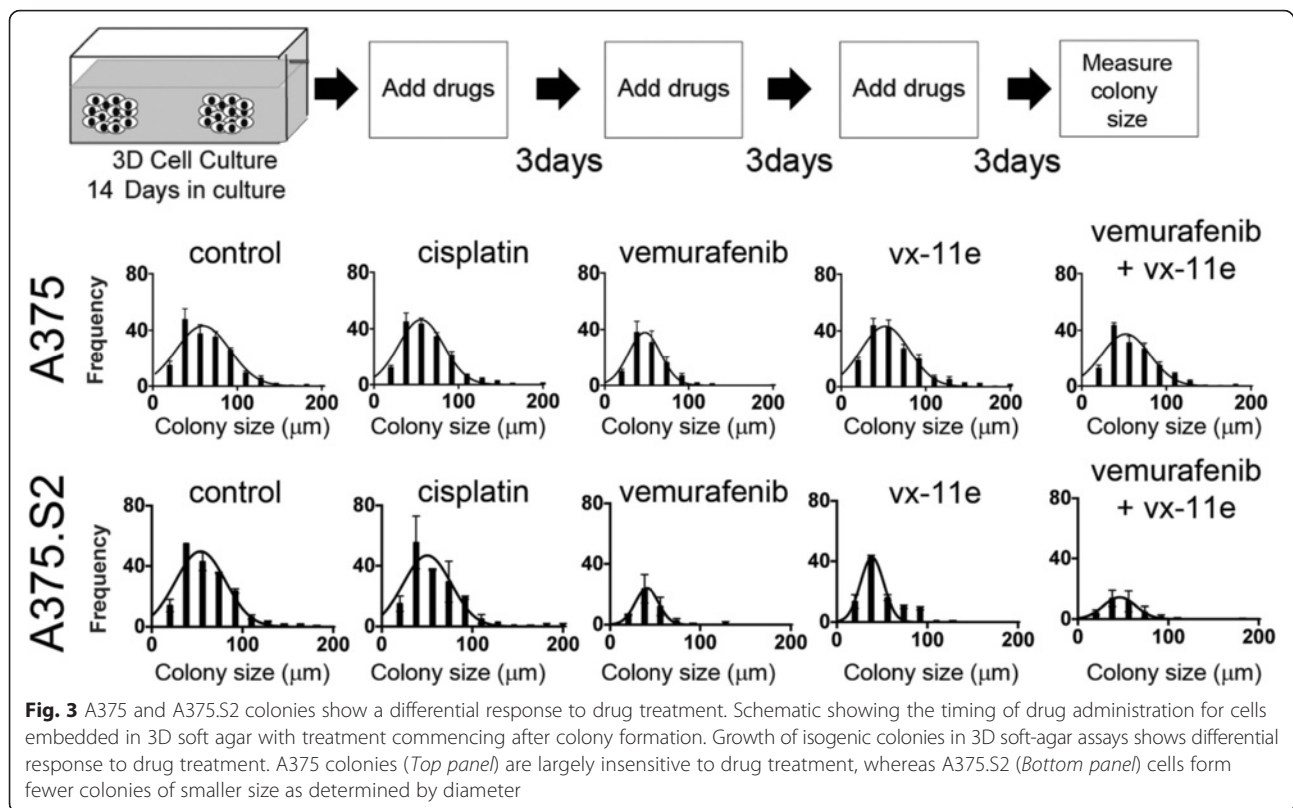
FN deposition is increased in metastatic melanoma cells
 Immunoblots of proteins extracted from cell lysates (CL) and conditioned media (CM) show that the A375 cells secreted less FN than the A375.S2 cells when they were cultured in 2D environment (Fig. 2a). We confirmed these cell lines express FN1 via RT-PCR (Additional file 1: Figure S1b). When these cell lines were cultured in laminin-rich ECM (lrECM), a complex matrix more closely mimicking in vivo conditions, both cell lines secreted more FN than in 2D culture (Fig. 2a). The A375 cells formed large, irregular “grape-like” aggregates, whereas A375.S2 clone formed smaller compact “masses” (Fig. 2b). The mean cross-section area and circularity of the A375.S2 colonies were significantly different from the A375 colonies (Additional file 1: Figure S1c). These differences in morphology and shape were similar to phenotypes observed for 3D culture of breast



tumor cells [25]. Additionally, confocal immunofluorescence revealed that cells secreted FN and assembled FN-globular networks in 3D lrECM culture, in contrast to the fibrils observed in 2D culture (Fig. 2b). The immunofluorescence of colonies grown in soft agar further confirms that both clones can assemble FN structures in a foreign microenvironment, and that this FN is tumor-derived (Fig. 2c). To establish the relevance to human disease progression, we determined that FN levels vary as a function of malignancy in human tissue arrays. Compared to normal skin and non-metastatic melanoma, we observed increased FN deposition at sites of melanoma metastasis (Fig. 2d). FN deposition was specifically localized to the metastatic lesions rather than adjacent normal lung or lymph epithelium.

Difference in tumor architecture affects MAPK inhibitor sensitivity

Tumor architecture has been shown to be an important factor for determining drug responses in breast tumors cultured in 3D lrECM compared to the tissue culture [28]. To determine whether the efficacy of drugs targeting the MAPK pathway may be similarly governed by tissue architecture, we recreated an established tumor and drug regimen using a 3D soft agar assay, in which we administered drug treatment once every three days. This time frame was designed to establish tumors that lacked necrotic cores. Then we administered drug treatment that mimics clinical settings (Fig. 3 Top panel). Colonies derived from A375 cells were largely insensitive to cisplatin, vemurafenib, vx-11e and vemurafenib + vx-



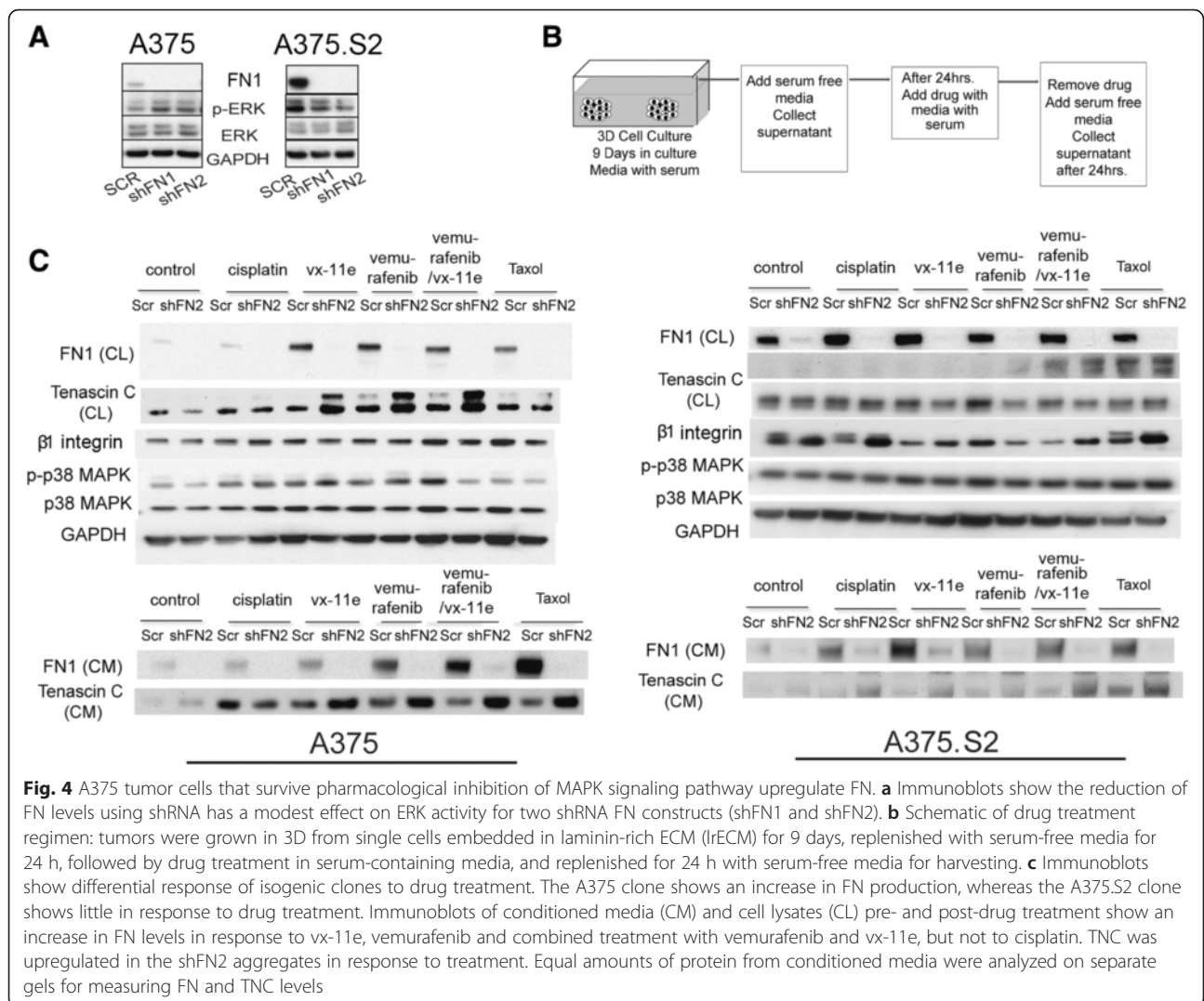
11e co-incubation. Contrary to A375 cells, the A375.S2 colonies showed increased sensitivity to drugs targeting the MAPK signaling pathway as determined by a reduction of number of colonies concomitant with reduced colony diameters (Fig. 3 Bottom Panel).

We reasoned that the ability to modulate FN secretion might mediate survival in the parental clone as compared to the A375.S2 cells. To determine if heterogeneity in FN deposition mediated the observed differential drug sensitivity between the clones, we generated two stable cell lines, named shFN1 and shFN2, producing reduced levels of FN using two shRNAs, respectively. In addition, a scramble control (Scr) was made. These three cell lines were cultured in 3D using soft agar for 21 days before protein extraction. Immunoblots revealed that an approximately 80 % reduction of FN protein was found in shFN1 and shFN2 cell lines, compared to the Scr cells. However, the shFN1 and shFN2 cells did not show significant difference in ERK activation (Fig. 4a). To determine if cell-ECM crosstalk was impaired with reduced FN biogenesis, we examined expression of integrins that facilitate cross talk with FN, and modulate cellular attachment to the ECM *in vivo*. Comparing the shFN1 and shFN2 cells, α v integrin expression was different but β 1 integrin was not (Additional file 1: Figure S2). Besides, shFN1 and shFN2 cells expressed higher levels of β 1 integrin than the wildtype and Scr counterparts,

while FN knockdown did not affect α v integrin expression level (Additional file 1: Figure S2). This highlights that shFN cells maintain the machinery for cell-ECM communication, and suggests that β 1 integrin levels correlate with FN modulation. Similarly, we asked if altered cell cycle progression may account for differential sensitivity. We determined that the cell cycle was unchanged in shFN cells compared to Scr cells (Additional file 1: Figure S3).

FN deficiency increases Tenascin-C

We next examined the secretome profiles of cells cultured in 3D IrECM. Culture medium from A375 and A375.S2 cells were collected before and after drug treatment (Fig. 4b). In A375 Scr cells, FN was found to increase at the cellular level in response to vx-11e, vemurafenib and paclitaxel treatments (Fig. 4c- Left panel). The surviving population tuned FN biogenesis under stress, particularly noting the dramatic increase following BRAF and ERK inhibition, but not for cisplatin and paclitaxel. FN-deficient aggregates, on the other hand, showed upregulation of Tenascin-C (TNC) in response to drug treatment. In contrast, the A375.S2 cells showed only a modest response despite displaying higher baseline levels of FN, which correlates with the reduced vitality of A375.S2 colonies cultured in agar (Fig. 4c- Right panel).



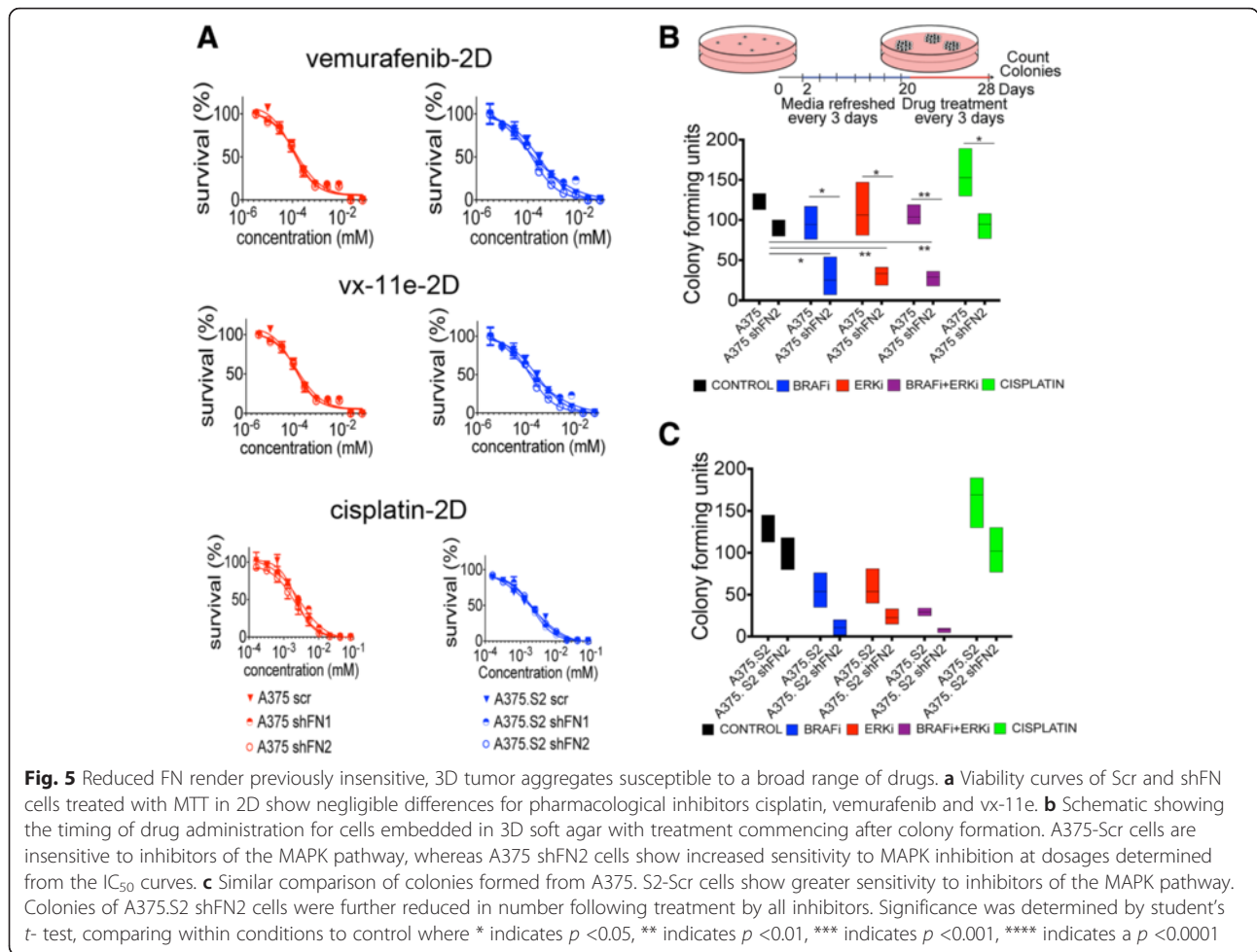
FN reduction sensitizes melanoma colonies to cisplatin, vemurafenib and Vx-11e

To determine whether FN reduction in melanoma cells could affect drug sensitivity, we assessed the sensitivity of the A375, A375.S2, with their Scr and shFN clones, with vemurafenib, vx-11e and cisplatin cultured in 2D and 3D environments. The half maximal inhibitory concentration (IC₅₀), as determined from the viability curves constructed post-MTT assay in 2D, remains unchanged despite the reduced levels of FN (Fig. 5a). By measuring cellular uptake of nitroretazolium blue chloride, we confirmed that the cells were metabolically active (Additional file 1: Figure S4B). However, we confirmed changes in intracellular signaling in response to treatment by assessing ERK activity in addition to MAPK activation (Additional file 1: Figure S4A), suggesting that observed sensitivity of FN-deficient colonies correlates with molecular events tied to 3D architecture establishment. Both Scr and shFN cell lines responded to

treatment when BRAF^{V600E} and ERK inhibitors were administered before colony formation (Additional file 1: Figure S4C). Interestingly, normal resistance to cisplatin observed in wild type malignant melanoma cells was diminished in the shFN cell lines in this assay. When cells were allowed to form colonies, those colonies derived from control Scr cells remained largely intact and insensitive to any of the drugs administered (Fig. 5b). shFN colonies were sensitive, showing a reduced number of surviving colonies following drug treatment (Fig. 5b). FN-depleted A375.S2 colonies showed an exaggerated sensitivity to drugs targeting MAPK signaling (Fig. 5c).

FN expression is part of signaling pathway in drug response

To understand the role of FN architecture in determining malignant melanoma tumor sensitivity to treatment, we sought to determine whether drug uptake was endogenously affected in shFN cells, or if assembly of



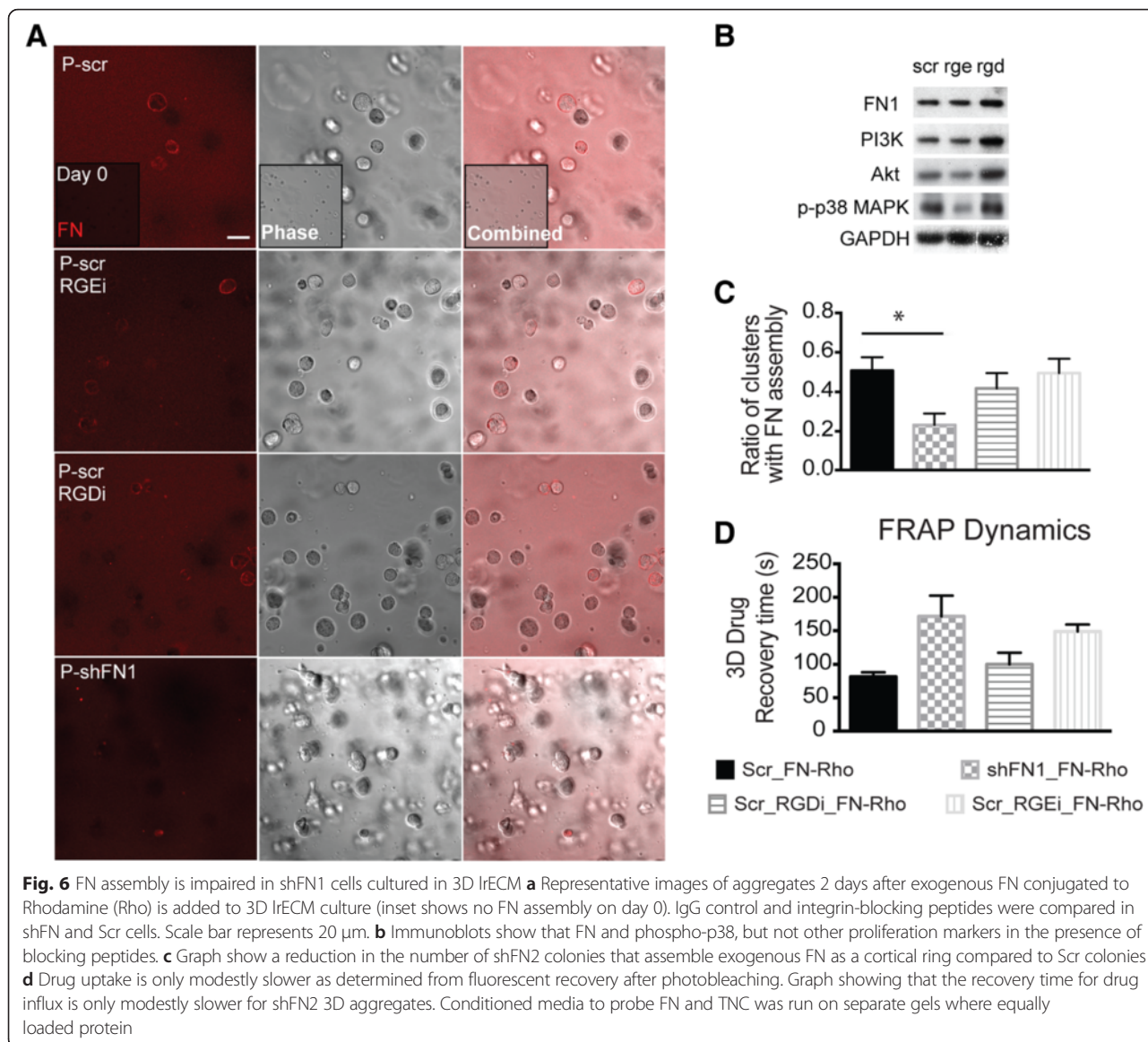
bioavailable fibronectin would rescue the observed sensitivity. First, we added exogenous fluorescent-labeled FN to Scr and shFN cells that were cultured in 3D rECM. As a further control, the Scr cell line was incubated with and without RGD motif-blocking peptides. We observed assembly of FN into *de novo* cortical rings formed 48 h post-addition by control cells (Fig. 6a). Immunoblots revealed that FN levels remained constant despite the presence of blocking peptides (Fig. 6b). However, fewer shFN aggregates assembled cortical FN (Fig. 6c). Using fluorescent conjugated taxol, we found that drug uptake in 2D culture was unaffected (Additional file 1: Figure S5), but fluorescence recovery after photobleaching (FRAP) in shFN 3D aggregates revealed that drug recovery time was modestly slower (Fig. 6d).

These data suggested in addition to providing a physical barrier, secreted FN might be part of an essential signaling cascade in responds to extracellular stress. We observed that p38 signaling was increased after drug treatment (Fig. 4c). Combined treatment with BRAF^{V600E} and p38 MAPK inhibitors consequently reduced FN secretion in Scr cells, and lowered TNC

expression in shFN cells (Fig. 7a). This suggests that p38 MAPK activity is necessary to fully upregulate FN (or TNC if FN production is impaired) in response to drug. Earlier we suggested a role for β1 integrin in similarly modulating FN biogenesis. Cells grown in the presence of β1 integrin-blocking antibody, BRAF and p38 inhibitors produce drastically less FN (Fig. 7b). p38 MAPK and β1 integrin inhibition prevented malignant melanoma cells from modulating FN expression, which was shown to be essential in surviving pharmaceutical stress.

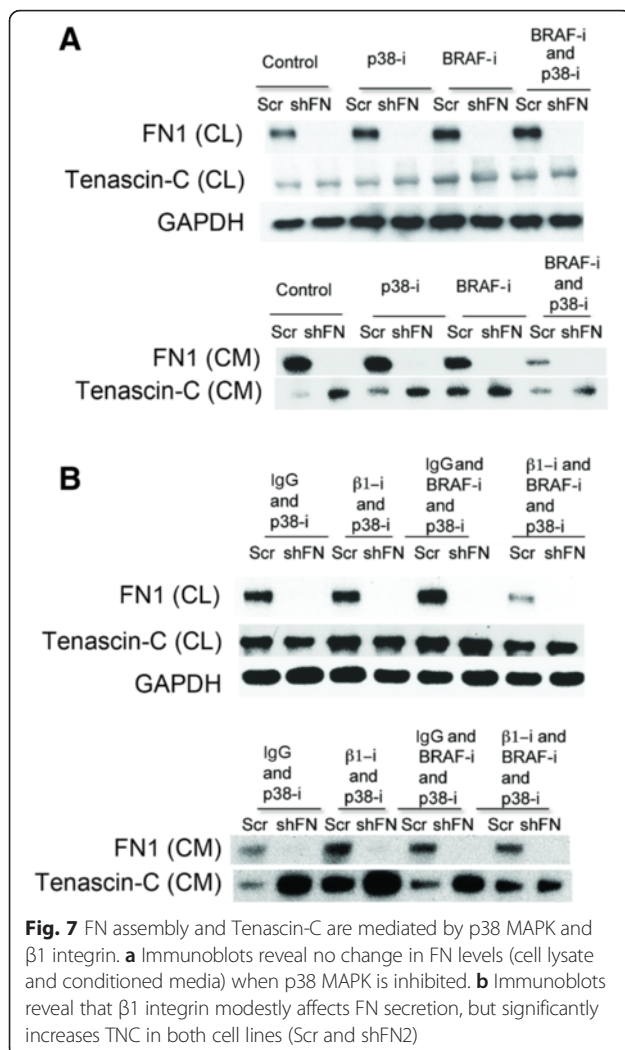
Discussion

Treatment strategies for metastatic malignant melanoma have significantly improved due to our current understanding of the molecular basis of tumor etiology [29]. Targeted therapy based on BRAF V600E status has yielded dramatic results and disease regression has been observed. In spite of recent progress, the stark reality is that current treatments do not yet achieve durable responses to melanoma intratumoral heterogeneity. The remodeling of the ECM results in changes within the microenvironment adding further complexity to the



determinants of drug efficacy and the likelihood of acquired resistance. We present a novel mechanism by which cells tune their ECM secretion, namely FN via p38 MAPK – β 1 integrin, in response to pharmaceutical inhibition of the MAPK signaling pathway in cutaneous melanoma cell lines, especially in 3D culture system. Here we show that when FN biogenesis is impaired, increased TNC expression is observed, suggesting a compensatory mechanism to attenuate drug treatment. By using the A375 cell lines that mimic tumor heterogeneity, we determined that only clones that can modulate FN biogenesis survive pharmaceutical intervention. These results, in conjunction with similar observations in patient data, suggest a role for ECM biosynthesis in the emergence of *de novo* resistance.

Extracellular matrix proteins (ECMs) are often observed to be abundantly expressed by tumor cells in comparison to their normal counterparts. Analysis of patient data confirmed that overexpression of ECM proteins such as FN and TNC are likewise observed in patients that had acquired *de novo* resistance from initial drug therapies. Similar outcomes have been noted for breast, laryngeal, urothelial and non-small-cell lung cancers [22, 30–32]. Using proteomics and immunofluorescence, we determined a distinct temporal distribution of secreted ECM components and visualized the assembled ECM scaffold for two isogenic malignant melanoma clones. We determined that melanoma cells modulate the secretion of many ECM proteins that are also implicated as potential biomarkers for patients suffering from metastatic disease [33]. Recently, ECM signatures were



assigned to breast and ovarian tumors of differing metastatic potential [34, 35]. These ECM signatures were not solely derived from the stromal cell secretions, but also included contributions from the tumor cells themselves [35]. Here, we go a step further to follow the evolution of a melanoma-derived ECM signature. In particular, the secretion patterns of the two clones were significantly different with respect to relative amounts of FN, perostin, TNC, laminins and vitronectin (Fig. 1c). FN also differed architecturally; fibrils were predominantly observed in one clone vs. globular scaffolds for the other (Fig. 2d). FN fibril assembly is regulated by tensional reorganization of actin via stress fibers for cells cultured in 2D [36–38]. Actin structures convey different mechanical properties based on spatial organization in 2D, and regulate specific motilities in 3D [25, 39]. Furthermore, cell motility regulates ECM remodeling and plays a role in the final architecture of the ECM scaffold [40]. These two cell lines show differential adhesion forces when placed in a 2D biomimetic platform simulating

cell-ECM interactions [41]. Additionally, differences in FN conformation dictate the availability of binding sites that affect signaling cascades associated with growth, migration and adhesion [42, 43]. In our system, it remains to be seen if there is a difference in tensional regulation and whether globular vs. fibril conformations show differential drug sensitivity.

In this study, we observed that FN was differentially secreted and assembled when tumor cells harboring the BRAF^{V600E} mutation were cultured in 2D vs. in a biomimetic 3D platform [44]. In vivo, tumor cells have access to various sources of fibronectin, namely the plasma and stroma. As a surrogate basement membrane gel, the laminin-rich ECM contains several ECM proteins and cytokines, including minute amounts of FN [40]. However, previous studies have shown that FN-null cells poorly assemble FN fibrils when exogenous FN is added to them [45]. We confirmed that a reduced number of shFN cells assembled exogenous FN compared to Scr cells in in vivo and in vitro 3D culture (Figs. 3 and 7). Growth inhibition when FN has been compromised has also been observed for other types of cancer [46]. This was due in part to reduced expression of β1 integrin and alterations of the cell cycle; however, in our system the short hairpin did not alter the cell cycle or reduce β1 integrin levels. Melanoma-derived conditioned media was shown to stimulate in vivo FN expression in target organs preceding future metastatic lesions. This phenomenon was also attributed to resident fibroblasts that create the “pre-metastatic niche” [47]. Our data suggests that metastatic melanoma also modulates its “tumor niche” by secreting and assembling its own ECM scaffold to survive drug treatment. Our results suggest that modulation of FN secretion serves as a response to external stress and may be separate from the remodeling of stromal components observed during initial malignant transformation.

Melanoma is largely resistant to platinum treatments since several factors such as drug uptake, increased efflux, extracellular interaction via cell adhesions and slow cycling cells may contribute to intrinsic resistance [48–50]. In our system 3D architecture did mitigate drug efficacy, as only a partial killing was achieved for FN-null tumor aggregates and minimal FN secretion was observed in response to cisplatin.

It has been previously reported that activation of the ERK/MAP kinase in melanoma cells stimulates FN biogenesis via the early growth response-1 transcription factor (Egr-1) [51]. High FN and Egr-1 levels were found in BRAF^{V600E} mutant cells and patient tumors. However, stimulation of the ERK pathway was insufficient to induce FN biogenesis in normal melanocytes [51]. Here, inhibition of the ERK pathway activates FN biogenesis via p38MAPK and β1 integrin signaling in melanoma

cells but not in melanocytes. In a previous study, β 1 integrin inhibition targeting FN has increased radio sensitization of breast tumor cells in 3D culture [52]. However, non-malignant breast cells undergo apoptosis following treatment with a β 1-integrin function-blocking antibody, whereas the malignant counterpart cells appear resistant to this treatment [53, 54]. Integrin blocking treatment is successful only if there is a differential response between normal tissue and its malignant counterpart. Thus, in addition to multiple targets of MAPK signaling, concomitant treatment with a p38 inhibitor may be a better strategy to prevent acquire drug resistance due to FN biosynthesis. However, in the case of metastatic disease, acute treatment with integrin-blocking antibodies may be useful to overcome *de novo* resistance. Nevertheless, alternative strategies to overcome FN mediated cell adhesion mediated drug resistance have been reported that could reverse drug resistance in leukemia and solid tumors [55, 56].

In normal cells during early embryogenesis, FN provides a scaffold for the assembly of other ECM proteins to direct organ specificity and fate, so we reasoned that other ECM proteins would be altered when FN biogenesis is affected [57]. In fact, we observed an increase in Tenascin-C biogenesis by shFN melanoma cells. Here, we show that drug treatment may induce ECM biosynthesis, contributing to *de novo* resistance. This must be considered when designing therapeutic interventions. Our findings suggest that modulation of tumor ECM biogenesis mimics the behavior of bacteria that assemble a biofilm in response to nutrient deficiencies, antibiotics and oxidative stress [58]. This biofilm acts as a physical barrier and signaling reservoir to communicate sensing of deleterious conditions. Tumor cells may use this secreted “biofilm” to communicate and communally enter a state of dormancy until environmental conditions are more favorable. If we can understand the mechanisms underlying tumor biofilm assembly, we may be able to seize a novel opportunity for therapeutic intervention.

Conclusions

In this study, we observed an increase in Tenascin-C biogenesis in melanoma cells expressing reduced level of fibronectin, suggesting a compensatory mechanism in response to drug treatment. We also showed that drug treatment could induce ECM biosynthesis, contributing to *de novo* resistance. Our findings suggest that modulation of tumor ECM biogenesis mimics the behavior of bacteria that assemble a biofilm in response to nutrient deficiencies, antibiotics and oxidative stress.

Ethics approval and consent to participate

The data shown in Fig. 2b was generated by using publicly available RNAseq data from human patients. No

ethics approval and consent to participate documents are necessary.

Consent to publish

This manuscript does not contain data from any individual person's data in any form require consent to publish from that person, or in the case of children, their parent or legal guardian.

Availability of data and materials

The datasets supporting the conclusions of this article are included within the article (and its additional files).

Additional file

Additional file 1: Supplemental Figures. (PDF 1475 kb)

Abbreviations

ECM: extracellular matrix; FN: fibronectin; IrECM: laminin-rich ECM; MAPK: mitogen-activated protein kinase; TNC: tenascin-C.

Competing interests

The authors declare that they have no competing interests.

Authors' contribution

AA, AD, EC, HT, KF, WV, YK, BB, BBusby, and KT performed experiments and data analysis. AA, AD, EC, HT, KF, and KT wrote the main manuscript text, AA, AD, KF, and KT prepared figures. All authors read, reviewed and approved the final manuscript.

Funding

This research was supported by the Intramural Research Program of the National Institutes of Health, National Cancer Institute.

Author details

¹Laboratory of Cell Biology, Center for Cancer Research, National Cancer Institute, National Institutes of Health, 37 Convent Dr., Bethesda, MD 20892, USA. ²Laboratories of Genitourinary Cancer Pathogenesis, Center for Cancer Research, National Cancer Institute, National Institutes of Health, 37 Convent Dr., Bethesda 20892MD, USA. ³National Centers for Biotechnology Information, National Library of Medicine, National Institutes of Health, Bethesda 20892MD, USA. ⁴Proteomics Shared Resource at the Herbert Irving Comprehensive Cancer Center & Department of Pharmacology, Columbia University Medical Center, New York 10032NY, USA.

Received: 22 August 2015 Accepted: 22 February 2016

Published online: 05 March 2016

References

- Chin L. The genetics of malignant melanoma: lessons from mouse and man. *Nat Rev Cancer*. 2003;3(8):559–70.
- Davies H, Bignell GR, Cox C, Stephens P, Edkins S, Clegg S, et al. Mutations of the BRAF gene in human cancer. *Nature*. 2002;417(6892):949–54.
- Balch CM, Gershenwald JE, Soong SJ, Thompson JF, Atkins MB, Byrd DR, et al. Final version of 2009 AJCC melanoma staging and classification. *J Clin Oncol*. 2009;27(36):6199–206.
- Gogas HJ, Kirkwood JM, Sondak VK. Chemotherapy for metastatic melanoma: time for a change? *Cancer*. 2007;109(3):455–64.
- Dummer R, Flaherty KT. Resistance patterns with tyrosine kinase inhibitors in melanoma: new insights. *Curr Opin Oncol*. 2012;24(2):150–4.
- Flaherty KT, Puzanov I, Kim KB, Ribas A, McArthur GA, Sosman JA, et al. Inhibition of mutated, activated BRAF in metastatic melanoma. *N Engl J Med*. 2010;363(9):809–19.
- Hauschild A, Grob JJ, Demidov LV, Jouary T, Gutzmer R, Millward M, et al. Dabrafenib in BRAF-mutated metastatic melanoma: a multicentre, open-label, phase 3 randomised controlled trial. *Lancet*. 2012;380(9839):358–65.

8. McArthur GA, Chapman PB, Robert C, Larkin J, Haanen JB, Dummer R, et al. Safety and efficacy of vemurafenib in BRAF(V600E) and BRAF(V600K) mutation-positive melanoma (BRIM-3): extended follow-up of a phase 3, randomised, open-label study. *Lancet Oncol*. 2014;15(3):323–32.
9. Lin WM, Baker AC, Beroukhi R, Winckler W, Feng W, Marmion JM, et al. Modeling genomic diversity and tumor dependency in malignant melanoma. *Cancer Res*. 2008;68(3):664–73.
10. Flaherty KT, Infante JR, Daud A, Gonzalez R, Kefford RF, Sosman J, et al. Combined BRAF and MEK inhibition in melanoma with BRAF V600 mutations. *N Engl J Med*. 2012;367(18):1694–703.
11. Alcala AM, Flaherty KT. BRAF inhibitors for the treatment of metastatic melanoma: clinical trials and mechanisms of resistance. *Clin Cancer Res*. 2012;18(1):33–9.
12. Pratilas CA, Solit DB. Targeting the mitogen-activated protein kinase pathway: physiological feedback and drug response. *Clin Cancer Res*. 2010;16(13):3329–34.
13. Green SK, Frankel A, Kerbel RS. Adhesion-dependent multicellular drug resistance. *Anticancer Drug Des*. 1999;14(2):153–68.
14. Teicher BA, Herman TS, Holden SA, Wang YY, Pfeffer MR, Crawford JW, et al. Tumor resistance to alkylating agents conferred by mechanisms operative only in vivo. *Science*. 1990;247(4949 Pt 1):1457–61.
15. Damiano JS, Cress AE, Hazlehurst LA, Shtil AA, Dalton WS. Cell adhesion mediated drug resistance (CAM-DR): role of integrins and resistance to apoptosis in human myeloma cell lines. *Blood*. 1999;93(5):1658–67.
16. Frankel A, Buckman R, Kerbel RS. Abrogation of taxol-induced G2-M arrest and apoptosis in human ovarian cancer cells grown as multicellular tumor spheroids. *Cancer Res*. 1997;57(12):2388–93.
17. Bissell MJ, Radisky D. Putting tumours in context. *Nat Rev Cancer*. 2001;1(1):46–54.
18. Villanueva J, Herlyn M. Melanoma and the tumor microenvironment. *Curr Oncol Rep*. 2008;10(5):439–46.
19. Lal A, Lash AE, Altschul SF, Velculescu V, Zhang L, McLendon RE, et al. A public database for gene expression in human cancers. *Cancer Res*. 1999;59(21):5403–7.
20. Auersperg N, Kruk PA, MacLaren IA, Watt FM, Myrdal SE. Heterogeneous expression of keratin, involucrin, and extracellular matrix among subpopulations of a poorly differentiated human cervical carcinoma: possible relationships to patterns of invasion. *Cancer Res*. 1989;49(11):3007–14.
21. Anastassiades OT, Pryce DM. Fibrosis as an indication of time in infiltrating breast cancer and its importance in prognosis. *Br J Cancer*. 1974;29(3):232–9.
22. Eke I, Storch K, Krause M, Cordes N. Cetuximab attenuates its cytotoxic and radiosensitizing potential by inducing fibronectin biosynthesis. *Cancer Res*. 2013;73(19):5869–79.
23. Sethi T, Rintoul RC, Moore SM, MacKinnon AC, Salter D, Choo C, et al. Extracellular matrix proteins protect small cell lung cancer cells against apoptosis: a mechanism for small cell lung cancer growth and drug resistance in vivo. *Nat Med*. 1999;5(6):662–8.
24. Valsesia A, Rimoldi D, Martinet D, Ibberson M, Benaglio P, Quadroni M, et al. Network-guided analysis of genes with altered somatic copy number and gene expression reveals pathways commonly perturbed in metastatic melanoma. *PLoS One*. 2011;6(4):e18369.
25. Tanner K, Mori H, Mroue R, Bruni-Cardoso A, Bissell MJ. Coherent angular motion in the establishment of multicellular architecture of glandular tissues. *Proc Natl Acad Sci U S A*. 2012;109(6):1973–8.
26. Kaariainen E, Nummela P, Soikkeli J, Yin M, Lukk M, Jahnkola T, et al. Switch to an invasive growth phase in melanoma is associated with tenascin-C, fibronectin, and procollagen-I forming specific channel structures for invasion. *J Pathol*. 2006;210(2):181–91.
27. Sun C, Wang L, Huang S, Heynen GJ, Prahalad A, Robert C, et al. Reversible and adaptive resistance to BRAF(V600E) inhibition in melanoma. *Nature*. 2014;508(7494):118–22.
28. Weigelt B, Lo AT, Park CC, Gray JW, Bissell MJ. HER2 signaling pathway activation and response of breast cancer cells to HER2-targeting agents is dependent strongly on the 3D microenvironment. *Breast Cancer Res Treat*. 2010;122(1):35–43.
29. Wagle N, Emery C, Berger MF, Davis MJ, Sawyer A, Pochanard P, et al. Dissecting therapeutic resistance to RAF inhibition in melanoma by tumor genomic profiling. *J Clin Oncol*. 2011;29(22):3085–96.
30. Ioachim E, Charchanti A, Briasoulis E, Karavasilis V, Tsanou H, Arvanitis DL, et al. Immunohistochemical expression of extracellular matrix components tenascin, fibronectin, collagen type IV and laminin in breast cancer: their prognostic value and role in tumour invasion and progression. *Eur J Cancer*. 2002;38(18):2362–70.
31. Ioachim E, Michael M, Stavropoulos NE, Kitsiou E, Salmas M, Malamou-Mitsi V. A clinicopathological study of the expression of extracellular matrix components in urothelial carcinoma. *BJU Int*. 2005;95(4):655–9.
32. Pietruszewska W, Kobos J, Bojanowska-Pozniak K, Durko M, Gryczynski M. Immunohistochemical analysis of the fibronectin expression and its prognostic value in patients with laryngeal cancer. *Otolaryngol Pol*. 2006;60(5):697–702.
33. Erickson HP, Bourdon MA. Tenascin: an extracellular matrix protein prominent in specialized embryonic tissues and tumors. *Annu Rev Cell Biol*. 1989;5:71–92.
34. Cheon DJ, Tong Y, Sim MS, Dering J, Berel D, Cui X, et al. A collagen-remodeling gene signature regulated by TGF-beta signaling is associated with metastasis and poor survival in serous ovarian cancer. *Clin Cancer Res*. 2014;20(3):711–23.
35. Naba A, Clauser KR, Lamar JM, Carr SA, Hynes RO. Extracellular matrix signatures of human mammary carcinoma identify novel metastasis promoters. *ELife*. 2014;3:e01308.
36. Hynes RO, Yamada KM. Fibronectins: multifunctional modular glycoproteins. *J Cell Biol*. 1982;95(2 Pt 1):369–77.
37. Sechler JL, Schwarzbauer JE. Coordinated regulation of fibronectin fibril assembly and actin stress fiber formation. *Cell Adhes Commun*. 1997;4(6):413–24.
38. Ohashi T, Kiehart DP, Erickson HP. Dual labeling of the fibronectin matrix and actin cytoskeleton with green fluorescent protein variants. *J Cell Sci*. 2002;115(Pt 6):1221–9.
39. Tanner K, Boudreau A, Bissell MJ, Kumar S. Dissecting regional variations in stress fiber mechanics in living cells with laser nanosurgery. *Biophys J*. 2010;99(9):2775–83.
40. Tanner K. Regulation of the basement membrane by epithelia generated forces. *Phys Biol*. 2012;9(6):065003.
41. Blehm BH, Jiang N, Kotobuki Y, Tanner K. Deconstructing the role of the ECM microenvironment on drug efficacy targeting MAPK signaling in a pre-clinical platform for cutaneous melanoma. *Biomaterials*. 2015;56:129–39.
42. Klotzsch E, Smith ML, Kubow KE, Muntwyler S, Little WC, Beyeler F, et al. Fibronectin forms the most extensible biological fibers displaying switchable force-exposed cryptic binding sites. *Proc Natl Acad Sci U S A*. 2009;106(43):18267–72.
43. Schwarzbauer JE, DeSimone DW. Fibronectins, Their Fibrillogenesis, and In Vivo Functions. *Csh Perspect Biol* 2011, 3(7) doi: 10.1101/cshperspect.a005041.
44. Bristow RG, Hill RP. Hypoxia and metabolism. Hypoxia, DNA repair and genetic instability. *Nat Rev Cancer*. 2008;8(3):180–92.
45. Bae E, Sakai T, Mosher DF. Assembly of exogenous fibronectin by fibronectin-null cells is dependent on the adhesive substrate. *J Biol Chem*. 2004;279(34):35749–59.
46. Sengupta S, Nandi S, Hindi ES, Wainwright DA, Han Y, Lesniak MS. Short hairpin RNA-mediated fibronectin knockdown delays tumor growth in a mouse glioma model. *Neoplasia*. 2010;12(10):837–47.
47. Kaplan RN, Riba RD, Zacharoulis S, Bramley AH, Vincent L, Costa C, et al. VEGFR1-positive haematopoietic bone marrow progenitors initiate the pre-metastatic niche. *Nature*. 2005;438(7069):820–7.
48. Roesch A, Vultur A, Bogeski I, Wang H, Zimmermann KM, Speicher D, et al. Overcoming intrinsic multidrug resistance in melanoma by blocking the mitochondrial respiratory chain of slow-cycling JARID1B(high) cells. *Cancer Cell*. 2013;23(6):811–25.
49. Stewart DJ. Mechanisms of resistance to cisplatin and carboplatin. *Crit Rev Oncol Hematol*. 2007;63(1):12–31.
50. Chen KG, Valencia JC, Gillet JP, Hearing VJ, Gottesman MM. Involvement of ABC transporters in melanogenesis and the development of multidrug resistance of melanoma. *Pigment Cell Melanoma Res*. 2009;22(6):740–9.
51. Gaggioli C, Robert G, Bertolotto C, Baillet O, Abbe P, Spadafora A, et al. Tumor-derived fibronectin is involved in melanoma cell invasion and regulated by V600E B-Raf signaling pathway. *J Invest Dermatol*. 2007;127(2):400–10.
52. Nam JM, Onodera Y, Bissell MJ, Park CC. Breast cancer cells in three-dimensional culture display an enhanced radioresponse after coordinate targeting of integrin alpha5beta1 and fibronectin. *Cancer Res*. 2010;70(13):5238–48.
53. Weaver VM, Petersen OW, Wang F, Larabell CA, Briand P, Damsky C, et al. Reversion of the malignant phenotype of human breast cells in three-

- dimensional culture and in vivo by integrin blocking antibodies. *J Cell Biol.* 1997;137(1):231–45.
54. Weaver VM, Bissell MJ. Functional culture models to study mechanisms governing apoptosis in normal and malignant mammary epithelial cells. *J Mammary Gland Biol Neoplasia.* 1999;4(2):193–201.
 55. Matsunaga T, Fukai F, Miura S, Nakane Y, Owaki T, Kodama H, et al. Combination therapy of an anticancer drug with the FNIII14 peptide of fibronectin effectively overcomes cell adhesion-mediated drug resistance of acute myelogenous leukemia. *Leukemia.* 2008;22(2):353–60.
 56. Nakagawa Y, Nakayama H, Nagata M, Yoshida R, Kawahara K, Hirose A, et al. Overexpression of fibronectin confers cell adhesion-mediated drug resistance (CAM-DR) against 5-FU in oral squamous cell carcinoma cells. *Int J Oncol.* 2014;44(4):1376–84.
 57. Darribere T, Kotliansky VE, Chernousov MA, Akiyama SK, Yamada KM, Thiery JP, et al. Distinct regions of human fibronectin are essential for fibril assembly in an in vivo developing system. *Dev Dyn.* 1992;194(1):63–70.
 58. Berk V, Fong JC, Dempsey GT, Develioglu ON, Zhuang X, Liphardt J, et al. Molecular architecture and assembly principles of *Vibrio cholerae* biofilms. *Science.* 2012;337(6091):236–9.

Submit your next manuscript to BioMed Central and we will help you at every step:

- We accept pre-submission inquiries
- Our selector tool helps you to find the most relevant journal
- We provide round the clock customer support
- Convenient online submission
- Thorough peer review
- Inclusion in PubMed and all major indexing services
- Maximum visibility for your research

Submit your manuscript at
www.biomedcentral.com/submit

